STUDY OF MATERIALS FOR REACTORS EMPLOYING MOLTEN FLUORIDE SALTS OR PB-BI COOLANT USING AN ELECTRON IRRADIATION TEST FACILITY

V.M. Azhazha, O.S. Bakai, I.V. Gurin, I.M. Neklyudov, A.A. Omelchuk, V.F. Zelenskiy
National Science Center Kharkiv Institute of Physics&Technology, 61108 Kharkiv, Ukraine;
Frank Garner
Pacific Northwest National Laboratory, Box 999, Battelle Boulevard, Richland WA,
99352, USA

Overview of results obtained within the framework of the STCU Project #294 is given.

1. INTRODUCTION

The experience in development and use of the nuclear energy for more than a half of century brought us, as it had to be, good and bad news. Advantages of the atomic energy industry are:

−   low, as compare to fossil fuel sources, price of energy;
−   low level of pollutions and environmental contaminations;
−   large amount of available nuclear fuel;
−   developed, investigated and applied in industry advanced fuel elements, structural materials, technologies and safety securement for atomic power engineering is a good base for the further advance of the nuclear power engineering.

The most significant disadvantages of the nuclear power are:

−   increasing amount of the stored nuclear waste, highly toxic radionuclide, including military Pu and other minor actinides (MA);
−   radioactive contaminations of the environment due to the nuclear industry and accidents and disasters on the nuclear stations;
−   lack of strict control proliferation of the nuclear materials around the world inspite of serious efforts by international institutions to restrict this process. The main difficulty of the non-proliferation activity is connected with the fact that the declared peaceful use of the nuclear energy allows to store military Pu and other fissile materials which can be used in "pure" and "dirty" bombs.

One can see that advantages and disadvantages are of a global scale. They cannot be ignored or postponed and transferred to the next people generations without proper solutions. Fast exhausting of gas and oil makes the problems extremely sharp. Evidently that a proper solution has to be found in historically short time. It worth to note that the problems of nuclear power industry in Ukraine have additional specification. Many nuclear stations were built and are in use in Ukraine providing nearly half of the electric energy generation. Production of main nuclear fuel constituents, powerful metallurgical industry, advanced scientific and technological base of Ukraine were tightly incorporated in the nuclear industry of USSR. Nowadays the processing of the nuclear fuel cycle as well as industry of used nuclear fuel storage and reprocessing is on a very beginning development stage in our state. For this reason an optimal roadmap for nuclear energetic development in Ukraine for short-range and long-range time has to be developed taking into account results of the global evolution in this field and using existing industrial and scientific links and collaboration.

Recently an international community elaborated a Technological Roadmap for Generation IV Nuclear Systems (G-IV) [1]. Concepts of the next generation nuclear systems are proposed also in other projects [2,3]. It includes description of an optimal nuclear strategy and considerations and estimations of several projects of the nuclear reactors of the next generation. New ideas on fission fuel cycle, nuclear transmutation, use of the released energy and ecological safety are formulated. The most general ideas which one can meet in the project in different combinations are following:

1) Considerably higher, than in the reactors of current generation, outlet temperature, $600\ldots1200\ {}^{\circ}C$. Due to this feature generation of hydrogen, as an ecologically pure fuel, in thermo chemical and electrochemical cycles becomes possible.
2) Accelerator driven systems (ADS) are most probable candidates for G-IV. Subcritical, with neutron reproducing coefficient $\kappa \approx 98$, reactors can successfully be used with external neutron sources. Necessitated 2% of the neutrons will be generated by proton (or electron) beams projected on a liquid metallic target. Molten Pb, Pb-Bi eutectic (PBE) or Hg are considered as possible candidates for the target.
3) Metallic melts (Pb,PBE, Na) look like attractive coolants. In opposite to gaseous coolants (e.g. He) the metallic melts are efficiently operating at low pressures. Especially interesting are Pb and PBE because they are not as chemically aggressive as Na in a case of leakage.
4) Fluid fuel (in form of molten fluoride salts) is considered as a promising non-traditional fuel

ВОПРОСЫ АТОМНОЙ НАУКИ И ТЕХНИКИ. 2005. №4.
Серия: Физика радиационных повреждений и радиационное материаловедение (87), с. 3-19.

3

in several projects. Use of the fluid fuel simplifies the fuel processing and reprocessing cycle.

A worth noting is that a minor experience in long-term use of components and prototypes of the G-IV systems is stored. Some data are obtained and used systems are molten salts reactors constructed and tested in Oak-Ridge (see [4-6] and refs. quoted) fast reactors with Pb and PBE coolants designed and used in submarines and satellites in USSR and Russia [7,8]. But this experience is not enough for designing of constructions and use of the proposed G-IV reactors for a long time.

A key problem of the G-IV program is R&D of construction materials compatible with molten salts and Pb and PBE melts at high temperatures. A brief summary of the state of the art materials for the nuclear systems of the next generation is given in ref. [9]. Ni-Mo alloys (Hastelloys) were used in MSR [4-6] and ferritic-martensitic chromium steels were applied in reacrors with Pb and PBE [7,8]. The experimental data obtained show which way of the advanced materials designing is promising but we are staying at the very beginning of this way.

The STCU Project 294 (approved for financing on March 1st 2003) is devoted to designing and test of materials for MSR and ADS. Promising construction materials have to be tested in reactors using special loops reproducing all conditions of real MRS and ADS. Experiments of this type take a lot of time and need special technique and testing procedures An idea to imitate reactor conditions using e.g. electron or proton and irradiation for material tests is not a new one. Many important results of the nuclear science where got by this way. But it is well known that there are no proper scaling laws allowing to predict material behavior in reactor condition on the base of data obtained at different temperatures, irradiation fields, doses and dose rates. It is because of strong connection of different cooperative processes in solids under irradiation due to large local non-equilibrium generated by radiation damages. Nevertheless the nature of kinetic processes induced, modified and activated by irradiation on microscopic level are very similar independently on the type of irradiation. For this reason investigations of the kinetic processes under electron irradiation gives a valuable information which can be used for prediction of the material behavior in reactors using a proper rescaling of the kinetic coefficients.

A special remark concerning the corrosion kinetics in surface layers has to be made. The corrosion is controlled by chemical reactions. The reaction rate is rather sensitive to the local energy deposition due to irradiation. The irradiation excites electron states and can produce atomic replacements and displacements. These radiation induced elementary processes need excitation energy from one to some tens of eV per atom. Accelerated electrons and γ-quanta are ideal agents for activation of this processes. Therefore an electron accelerator of a proper energy (10 MeV per electron) was chosen to imitate impact of the reactor irradiation on the corrosion kinetics. In parallel, the electron irradiation impacts diffusion and phase transformations in bulk and, especially, within the grain boundaries. This general idea was used as basic one in planned within the framework of the Project 294 investigations.

It is worth to note that the performed corrosion tests in metallic melts and salts without irradiation not only provide a reference data base but allow estimating thermodynamic driving forces controlling the corrosion and aging kinetics.

To realize the project a methodology of tests was developed in detail and tested materials were chosen (see below). Really we have performed pilot experiments which have to be continued in larger scale but they allowed to get an important information on impact of electron and γ-irradiation on corrosion, compositional and mechanical properties of the tested materials.

In this overview paper we summarize and discuss the main results obtained within the framework of the Project. In detail the results obtained are presented in separated papers of this issue. Purposive goal of the overview is to describe concepts, methodology and to consider the main results obtained in their interconnection.

2. METHODOLOGY
2.1. ELECTRON IRRADIATION TEST FACILITY (EITF)

Main reasons for use electron irradiation for investigation of the radiation effect on materials for MRS and ADS are formulated in Introduction. Some features of the electron irradiation which are helpful in this kind of investigations are following:

1. Because energetic thresholds of nuclear reactions induced by electrons and γ-rays are nearly 10MeV or something less, use of the electron beams of 10M eV energy excludes considerable radioactivity of the irradiated materials. For this reason hot cells are not needed in postirradiation investigations of the materials.

2. The penetration length of electrons with 10 MeV energy is of some centimeters. On this scale of length the electron energy decreases from 10 to 1 MeV or even less due to bremsstrahlung and another inelastic processes. It means that, from one side, the test ampoules can have reasonable size to mimic large scale experiments and, from other side, the irradiation conditions are dramatically changing on comparatively small length. Therefore we can use many specimens of sub millimeter thickness within one ampoule to investigate dependence of corrosion and radiation damage processes versus energy deposited by e- and γ- fields.

3. The electron beam can be used as an efficient heater of the irradiated target, to keep a needed temperature if the electron beam power, target geometry and construction are chosen by a proper way.

The EITF construction [10] is shown in Fig.1. It was designed taking into account calculations of the e- and γ- fields as well as calculations of the thermal balance and temperature field [11].

ВОПРОСЫ АТОМНОЙ НАУКИ И ТЕХНИКИ. 2005. №.4.
Серия: Физика радиационных повреждений и радиационное материаловедение (87), с. 3-19.

4

2.2. SIMULATIONS OF THE *e*- AND γ - FIELDS AND DEPOSITED ENERGY DISTRIBUTION

The electron and γ -radiation fields, the deposited energy profiles in salt and samples as well as the point defects generation in Haselloy have been calculated by means simulation of the radiation transport in the test bench geometry [11]. The computer code based on the CERN GEANT4 Monte Carlo toolkit [13] was used for this simulation. The results of simulations are needed for optimization of the ampoule construction as well as for obtaining quantitative dependencies of the specimen properties on the dose.

2.3. TEMPERATURE DISTRIBUTION

Equation of the heat balance taking into account the integral deposited energy and the heat irradiation from the surface is a base for estimation of the temperature balance of irradiated target in total. To calculate temperature field within an ampoule the deposited energy distribution and heat transport equations have to be deduced and solved [12]. The temperature distribution is an important characteristic of the irradiated target. In our experiments the goal was to make this distribution as homogeneous as possible. The calculations performed show that the temperature variance is really small [12].

2.4. MECHANICAL TESTS

Changes of macroscopic mechanical properties due to impact of the molten fluoride salts or metallic coolants can be revealed by standard mechanical tests [14]. Because these changes are caused by structural alternations and, first of all, by alternations of the grain boundaries and dislocational system, as well as by compositional heterogeneities. Therefore systematic microindentations and nanoindentations of the materials in the vicinity of surface and in bulk were performed. Nanoindentations allow to measure local value of Young modulus which is sensitive to local compositional and structural changes [15].

Mechanical tests with impact of ultrasonic vibrations on the been tested material are of special interests because from one side they give information on the activated slipping of dislocations and, from another side, plastic deformation of vibrating or shocked elements of the reactor construction can be very different as compare to that without vibrations. Within the project framework a home-made device for mechanical tests under ultrasonic impact was designed and constructed [16].

In combination with metallography and microanalysis these methods are rather informative.

2.5. MICROANALYSIS

Compositional and phase changes can be revealed by mean of microanalysis. It is important to to reveal these changes on all scales in surface layers and in bulk of the tested materials. The X-ray phase analysis was performed on a DRON-UM diffractometer (CuKα-radi-

ation), the atomic absorption analysis on a Pionicum SP-9 spectrophotometer, the IR spectroscopic investigations on a Specord 80M instrument, the X-ray microanalysis and visual control of the state of the sample surface on a REM-101M scanning electron microscope-microanalyzer. Secondary ion mass spectrometry (SIMS) also was used to detect compositional changes in surface layers of tested samples [17, 18]. Microanalysis by mean of high resolution transmission electron microscopy is in progress.

2.6. CORROSION TESTS

The corrosion of alloys and their constituents in a molten eutectic sodium fluoride-zirconium fluoride mixture has been studied by cyclic voltammetry, X-ray analysis, scanning electron microscopy and metallography. The corrosion rates of the samples exposed in salt at 650 °C for different times were measured afterward in a fresh molten salt by the voltamperic method. Impact of electron irradiation on the corrosion rate of the alloys in molten fluorides has been investigated [15, 19].

2.7. ROENTGEN SPECTROSCOPY

After irradiation by 10MeV electrons a small account of nuclear reactions leading to formation of γ - active nuclei happens. Therefore a possibility to reveal products of the alloys corrosion in molten salt under irradiation exists. Inspite this method does not produce a proper quantitative compositional analysis it gives a semiquantitative and qualitative information [20].

2.8. THEORETICAL MODELS

For quantitative analysis of the experimental data appropriate theoretical models have to be developed. Main goal of these model is to describe corrosion kinetics and phase transformation kinetics taking into account impact of electron irradiation. Refs. [21, 22] are devoted to this problem solution.

2.9. THERMODYNAMICS OF ZR IN ALKALI HALIDE MELTS

Equilibrium constants determine the thermodynamic driven forces responsible for chemical reactions and dissolution of alloys. Because Zr and alkali metals are basic elements of all used fluoride salts of MSR, it is worth to know their thermodynamic characteristics. Investigations of the thermodynamics of Zr in alkali melts are performed within the framework of this project [23].

3. MATERIALS
3.1. HASTELLOYS

Ni-Mo alloys (Hastelloys) showed a satisfactory corrosion resistance in contact with molten fluoride salts ZrF_4 -NaF and ZrF_4 -LiF-BeF at temperatures 600… 800 $^\circ C$ [4-6]. It was revealed that comparatively small compositional changes of alloys can lead to consider-

ВОПРОСЫ АТОМНОЙ НАУКИ И ТЕХНИКИ. 2005. №.4.
Серия: Физика радиационных повреждений и радиационное материаловедение (87), с. 3-19.

5

able decrease or increase of the corrosion resistance. For example alloying with a few percents of Nb improves the corrosion resistance of the alloy. In [5] is proposed an "optimized" composition of Ni-Mo alloy that showed acceptable radiation resistance under neutron irradiation up to dose $\sim 10^{20}$ n/cm^2 . The data obtained [4-6] can serve very much as a starting point and background in further R&D materials compatible with fluoride molten salts at temperature above $600\,^{\circ}C$. Therefore for the corrosional tests of Ni-Mo alloys we have chosen the alloys of two compositions (alloy A and alloy B, see Table 1) that are very similar to those reported in Refs. [5]. In the Table 1 also the composition of alloy U which was tested under neutron irradiation is presented. The compounds of high purity were used to exclude impact of uncontrolled impurities. It has to be noted that microscopic mechanisms of the structural and compositional changes of Hastelloys in the molten salts under and withoutirradiation were never studied in detail. Very scant information about precipitations and heterogeneities of these alloys is available.

Table 1

Compositions of alloys A, B, and U

Element	Composition (wt %),		
	Alloy A	Alloy B	Alloy U
Nickel	78.2	78.2	78.2
Molybdenum	11.7	11.7	11…12
Chromium	6.7	6.2	5…7
Titanium	0.5	0.5	0.5
Aluminum	0.8	0.8	0.8…1.2
Iron	1.5	1.5	1.5
Manganese	0.5	0.5	0.5
Silicon	0.15	0.15	0.15
Niobium	-	0.5	0.5
Yttrium	-	0.05	-
Carbon	-	-	0.038
Sulfur	-	-	0.012

3.2. W AND Mo COVERS

Hastelloys are corroding very fast in molten Pb, PbE and Bi because these melts are good dissolvent for Ni. Ferritic/martensitic (F/M) chromium steels with oxided surface and steels covered by W or Mo are considered as materials with much better corrosion resistance in the mentioned melts. Beside W and Mo have small solubility in Pb and one can expect that these metals can be used as acceptable constitutive materials compatible with Pb abd PbE.

In NSC KIPT are developed different efficient technologies for covers formation. One of these technologies is suitable for W and Mo covers using thermolise of carbonyls of these metals. To make clear whether this technology provides W and Mo covers of a proper quality we have used the Hastelloy A as substrate. If these covers demonstrate good protective properties on this wittingly "bad" substrate, one can expect that they will be more efficient on (F/M) chromium steels which have an appropriate corrosion resistance by themselves. Up to now only corrosion resistance of alloy A covered by W

and Mo in molten ZrF_4 -NiF salt was studied and further experiments are planned.

3.3. CARBON-CARBON COMPOSITE

Different carbon materials are very useful in nuclear industry from very beginning. These materials can be used at high temperatures. Graphites are radiation resistant and have comparatively low chemical activity in contacts with fluoride salts [5]. Graphite has low mechanical properties what is a serious limitation for many applications. But C-C composites have much better mechanical properties. An original technology of C-C composite preparation is developed and efficiently used for different applications in NSC KIPT for many years. Tests of the corrosion resistance of these materials in molten salts under irradiation can give quantitative results on their corrosion properties.

4. RESULTS
4.1. HOME MADE DEVICES
4.1.1. ELECTRON IRRADIATION TEST FACILITY

EITF has been constructed and built at Linac-10 electron linear accelerator in NSC-KIPT (Fig. 1 and Fig. 2) [24].

Schematically construction of the ampoule is shown in Fig. 3 and Fig. 4.

A container assembly that consists of ampoules holding samples imbedded in fluoride salt is disposed in a chamber in Ar atmosphere. The container assembly includes 16 ampoules made of the C-C composite.

Electron beam with the 10 MeV energy and up to 1mA of average current (up to 1 kW of power) is in use. The electron beam is scanning over the chamber inlet window. The container assembly temperature is monitored with three thermocouples. The temperature is kept to be $(650ºC \pm 15)ºC$ and controlled by the beam current.
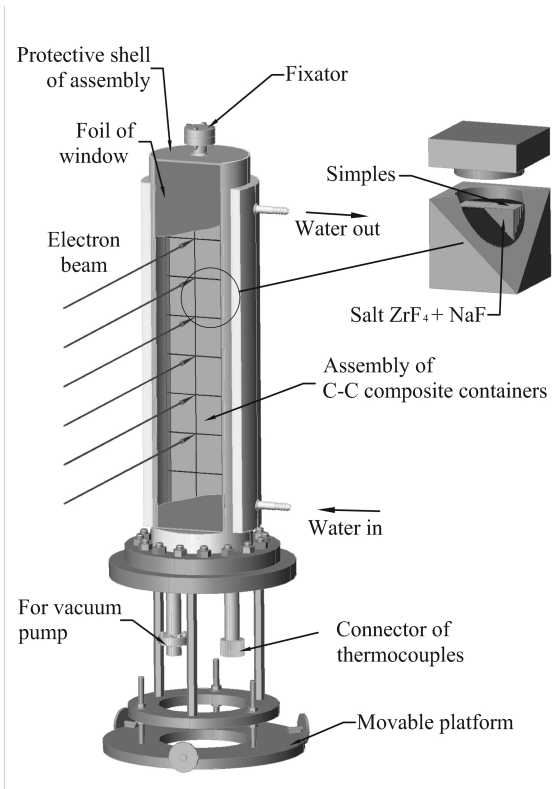
ВОПРОСЫ АТОМНОЙ НАУКИ И ТЕХНИКИ. 2005. №.4.
Серия: Физика радиационных повреждений и радиационное материаловедение (87), с. 3-19.

6

Fig. 1. Construction of the EITF-KIPT

Protective shell of assembly
Fixator
Foil of window
Simples
Electron beam
Water out
Salt ZrF$_4$ + NaF
Assembly of C-C composite containers
Water in
For vacuum pump
Connector of thermocouples
Movable platform
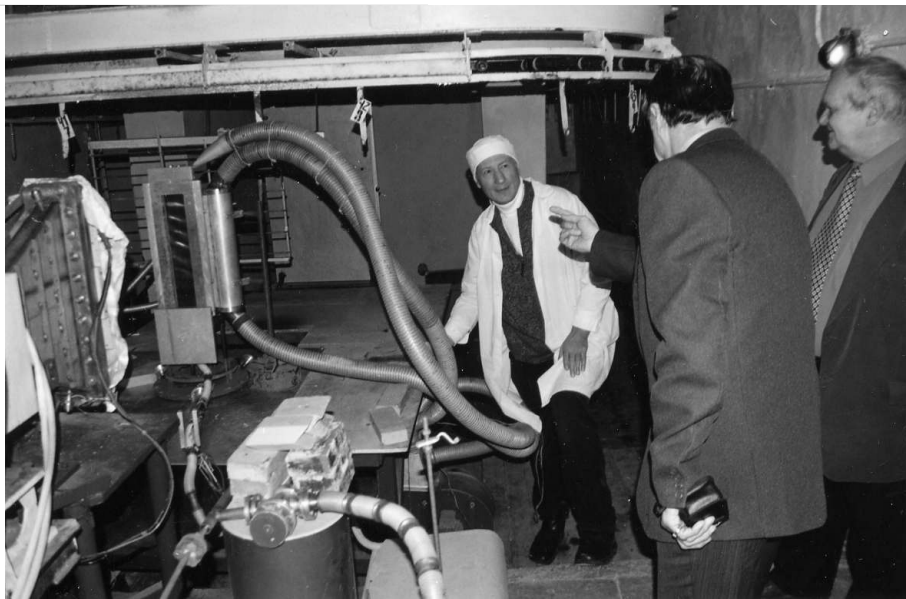
Fig. 2. General view of EITF
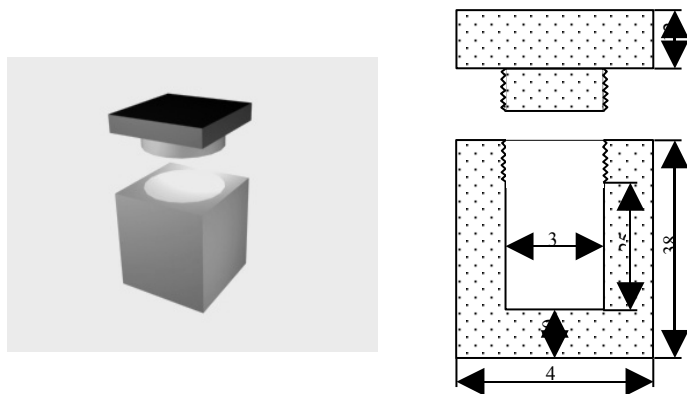
Fig. 3. Scheme of the ampoule construction

ВОПРОСЫ АТОМНОЙ НАУКИ И ТЕХНИКИ. 2005. №.4.
Серия: Физика радиационных повреждений и радиационное материаловедение (87), с. 3-19.

7
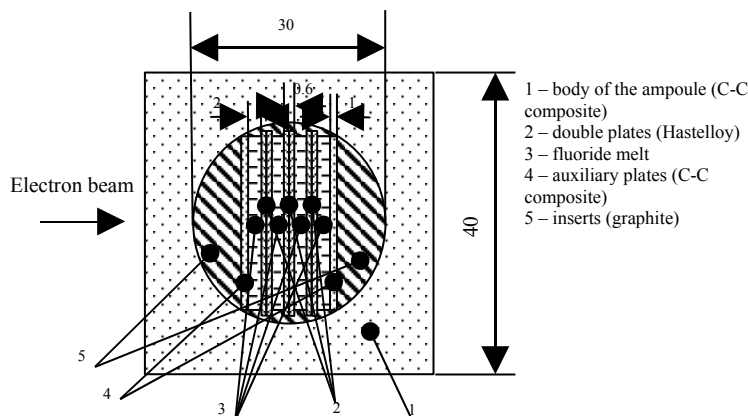
Fig. 4. Frontal section of the loaded ampoule

1 – body of the ampoule (C-C composite)
2 – double plates (Hastelloy)
3 – fluoride melt
4 – auxiliary plates (C-C composite)
5 – inserts (graphite)

4.1.2. ULTRASONIC MECHANICAL TEST FACILITY (UMTF)

The UMTF was designed and constructed for mechanical tests with impact of ultrasonic vibrations on the material [16]. A scheme of the UMTF is shown in Fig. 5. Ultrasonic vibrations are being generated by magnetostrictive converter and through concentrator focused on the tested specimen. The vacuum furnace allows to keep specimen temperature up to $1500\,^{\circ}C$. The ultrasound frequency range is 18…22 Khz. The ultrasonic generator has controlled power 2…4 kw but the transferred to specimen fraction of this power is yet not known. Storage of the measurement data will be made in digital form. Impact of the ultrasonic vibrations on the plastic deformation of irradiated and unirradiated specimens is planned.
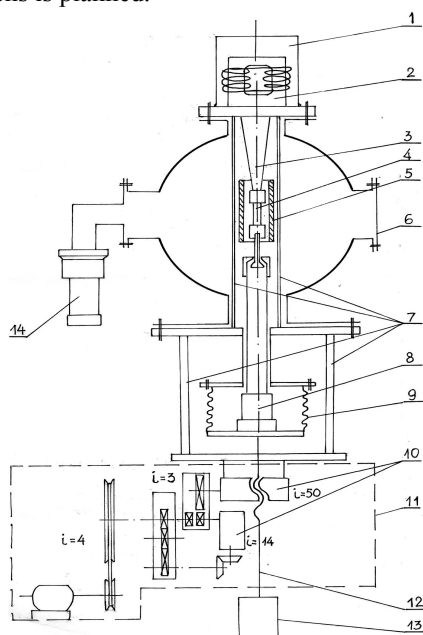
Fig. 5. Scheme of the USTF for mechanical tests under ultrasonic impact:
1. Water-jacket; 2. Magnetostrictive converter; 3. Ultrasound concentrator; 4. Specimen; 5. Vacuum furnace; 6. Flange; 7. Supportive blocks; 8. Dynamometer with piezometers of load; 9. Sylphon; 10. Worm gears; 11. Configuration of reduction system; 12. Feed spindle; 13. Dynamometer with piezometers of strain; 14. Diffusion vacuum pump

4.2. RESULTS OF SIMULATIONS OF THE e- AND γ - FIELDS AND DEPOSITED ENERGY DISTRIBUTION

To calculate the electron and γ-radiation fields, the deposited energy profiles in salt and specimens of Haselloy, the detailed Monte Carlo modeling was performed. The computer code based on the CERN GEANT4 Monte Carlo toolkit [13] was used for the simulation [11].

The results of the simulations were used for optimization of the ampoule construction. Namely, the number of specimens in the salt and their disposition within the ampoule were chosen to use the irradiating electron beam as efficiently as possible. Within the scope of the experimental geometry proposed the maximal variability of energy deposition on all interfaces of Hastelloy and molten fluoride salt is achieved. The modeling of complex multicomponent heterogeneous system of the assembled ampoule taking into account all valuable physical processes that determine the relativistic electrons energy deposition in substance provides information on the kinetics of development of electron-photon processes in this system. Results of the simulations allow obtaining quantitative dependencies of the specimen properties changes on the dose of deposited energy. The simulations data on data on depth profiles of the fluence and deposited energy are shown in Fig. 6. The digital data of these parameters and doses of the point defects (vacancies and interstitials) generations are presented in Table 2.

ВОПРОСЫ АТОМНОЙ НАУКИ И ТЕХНИКИ. 2005. №.4.
Серия: Физика радиационных повреждений и радиационное материаловедение (87), с. 3-19.
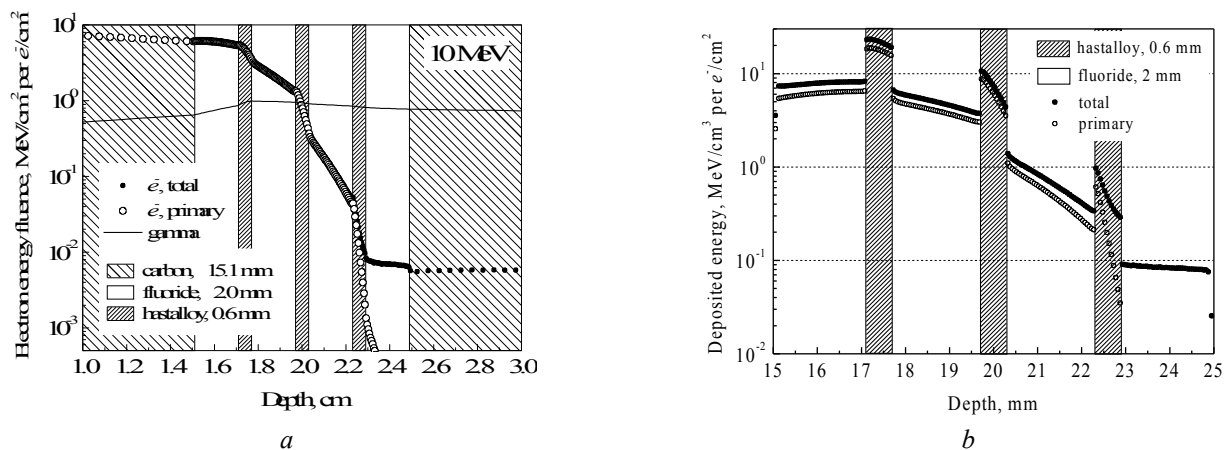
8

Fig. 6. Depth dependencies (a) of the particles normalized energy fluencies, incl. primary electrons and produced gammas, and (b) the deposited energy profile

The results of simulations were used for analysis of the dose dependencies of the corrosion stability and the mechanical properties of irradiated specimens. Besides the calculations of the temperature distribution within the ampoule are also based on these data.

It is seen that the energy deposited on the first surface (5066 eV/at) is two orders in magnitude larger than that on the last surface (63 eV/at) and that the deposited energy gradually decreases from the first to last surface.

The point defects generation dose is decreasing from 2.12×10^{-3} dpa within the first specimen to 4.42×10^{-6} dpa within the last one. Usually the ratio of the unstable Frenkel pairs to the stable ones is $\sim 10^2$. Therefore the irradiation induced replacements can modify the transport and segregation phenomena, especially in first and second specimens.

The deposited in the fluoride salt energy is several times less than that in the Hastelloy specimens. Nevertheless it is large enough to impact the chemical reactions within the salt.

Table 2

Deposited energies in the interface (near-surface) regions of the Hastelloy plates and the melt and atomic concentrations of Frenkel pairs in Hastelloy

Sample	Sample Surface	Material	Depth	Deposited Energy		Point Defects	
			cm	eV/atom	percentage	dpa	percentage
		fluoride	1.7075	2221.52			
1	1…1		1.7125	5066.72	100.0 100.0	2.12×10^{-3}	100.0 100.0
	1…2	Hastelloy	1.7375	4906.46	96.84 96.84	2.01×10^{-3}	94.44 94.44
2	2…1		1.7425	4815.29	95.04 95.04	1.95×10^{-3}	91.94 91.94
	2…2		1.7675	4208.23	83.06 83.06	1.62×10^{-3}	76.20 76.20
		fluoride	1.7725	1794.76			
			1.9675	1010.82			
3	3…1		1.9725	2347.23	46.33 100.0	7.00×10^{-4}	32.96 100.0
	3…2	Hastelloy	1.9975	1698.40	33.52 72.36	4.80×10^{-4}	22.59 68.54
4	4…1		2.0025	1563.33	30.85 66.60	4.33×10^{-4}	20.37 61.80
	4…2		2.0275	969.88	19.14 41.32	2.44×10^{-4}	11.48 34.83
		fluoride	2.0325	375.17			
			2.2275	90.93			
5	5…1		2.2325	214.55	4.23 100.0	2.75×10^{-5}	1.30 100.0
	5-2	Hastelloy	2.2575	107.01	2.11 49.88	1.06×10^{-5}	0.50 38.64
6	6-1		2.2625	95.04	1.88 44.30	8.83×10^{-6}	0.42 32.07
	6-2		2.2875	63.82	1.26 29.74	4.42×10^{-6}	0.21 16.07
		fluoride	2.2925	24.39			

The parameters of the irradiation effect on the salt and specimens for 700 hours exposure were estimated to be appropriate for investigations of the irradiation impact on corrosion and mechanical properties and compositional heterogeneities of hastelloy contacting with molten fluorides.

4.3. TEMPERATURE DISTRIBUTIONS

The calculations of the temperature distribution within the ampoule are based on the simulated distributions of the deposited energy distribution within ampoule reported in the previous section [12]. It is found

ВОПРОСЫ АТОМНОЙ НАУКИ И ТЕХНИКИ. 2005. №.4.
Серия: Физика радиационных повреждений и радиационное материаловедение (87), с. 3-19.

9

that the temperature variance within an ampoule is not more than 15°. This variance can be neglected when experimental data are analyzed.

4.4. RESULTS OF TESTS OF C-C COMPOSITE

There exists a big family of C-C composites differing in the fabrication technology and properties. In the tests performed we have used two types of the C-C composite differing in density of the surface layers. To make more dense composite an additional densification with pyrocarbon was used [25]. The tests performed show that exposure in the molten salt, without and under e-irradiation, and lead does not change properties and composition of the tested specimens and ampoules. It looks like the test conditions were not "hard" enough for this material.

In result of temperature cycling from room temperature to 600…700°C and isothermal soaking at high temperatures (for up to 700 h) it was shown [25] that C-C composite is impermeable to molten fluoride mixture and lead. This material is indestructible in an inert atmosphere and no considerable structure changes are revealed after 700 hours e-irradiation in inert atmosphere. It can be recommended for use in transmutation technologies.

Very eloquent are results of nanoindentations of the tested material. The results of the nanoindentations are presented in Table 3 and Fig. 7.

Samples of C-C composite were investigated without (sample 1) and with densification with pyrocarbon (samples 2). In samples 1, two constituents have been distinguished: fibers and binding material. The hardness and elastic modulus were determined from the depth of indentation according to the Oliver and Farr technique [26, 27]. A microscopic examination did not reveal indentations on the samples as this material has a high capacity for the elastic recovery of the original shape. This is evidenced by loading and unloading curves (Fig. 7).

Table 3

Mechanical properties of carbon-carbon composites

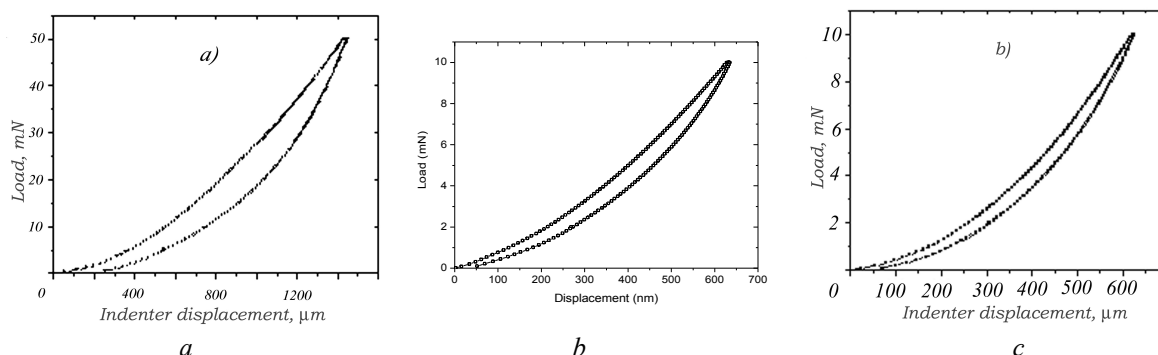| Sample	Elastic modules (GPa)	Hardness (Gpa)
Sample 1 (binding material)	17±2	2.83±0,14
Sample 1 (fiber)	19±1	2.11±0,23
Sample 1 (fiber)	17±0	1.72±0,38
Sample 2 (fiber)	20±2	2.72±0,35

Fig. 7. Loading and unloading curves for carbon-carbon composites (a) without contact with the fluoride melt and without irradiation; (b,c) after electron beam irradiation in a sodium fluoride – zirconium fluoride melt for 700 h at 650 °C: with deposited energy (b) (5066 MeV/atom) and (c) (64 MeV/atom)

The loading-unloading curves generally diverge on unloading. For the samples under investigation, these curves first diverge and then converge, and almost complete recovery of the original shape is observed on complete unloading. This character of dependencies and elastic modules are also the same as those of glassy carbon [27]. It looks like this material is a variety of glassy carbon (amorphous carbon in which sp^2 bonds predominated).

The hardness and elastic modules of the fibers and binding materials of the composites in samples 1 differ not so much what means that the mechanical properties are isotropic.

4.5. IMPACT OF ZRF₄− NAF MOLTEN SALT AND E-IRRADIATION ON PROPERTIES OF ALLOYS A AND B

4.5.1. METALLOGRAPHY

Metallography was used to reveal macroscopic structural changes of the tested specimens. In the case of a considerable intercrystalline corrossion (observed e.g. in refs [5,6]) it is clearly seen in form cracks and etched grain boundaries. The depth and density of the intercrystalline cracks can be used as a corrosion parameter [5]. Metallography of irradiated and unirradiated specimens in salt are shown in figs 12-15 [28].

In Fig. 8 a specimen of the alloy A exposed in salt at $T = 650°C$ for 700 hours is shown. The size of the grains is 60 μm. Precipitates in grain bulk and boundaries of some μm in size are seen. The specimen was not polished before the test and its roughness is not a result of corrosion. Attentive inspection of the grain boundaries shows that the depth of the "cracking" is not more than 1…3 μm.

ВОПРОСЫ АТОМНОЙ НАУКИ И ТЕХНИКИ. 2005. №.4.
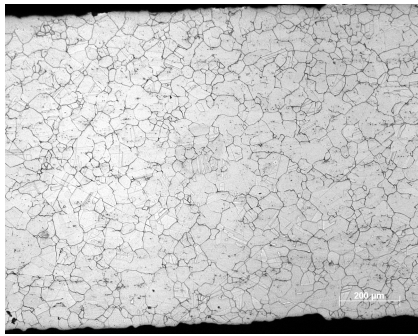*Серия:* Физика радиационных повреждений и радиационное материаловедение (87), с. 3-19.

10

Fig. 8. Structure of the Hastelloy A after 700 hr exposure in the molten salt at $T=650^{\circ}C$

Considerably different is morphology of the alloy A specimens irradiated in the molten salt for 700hr at $T=650^{\circ}C$ (Fig. 9). The depth of intercrystalline corrosion essentially depends on the deposited energy. The depth is 25…30 μm at $E_d=5066\,eV/at$ and 5…10 μm at $E_d=64\,ev/at$.

The statistics of precipitates of secondary phases is yet not considered quantitatively but the size of precipitates within grain boundaries are larger in irradiated material (Fig. 10).
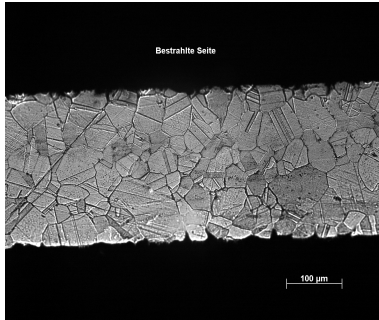
a
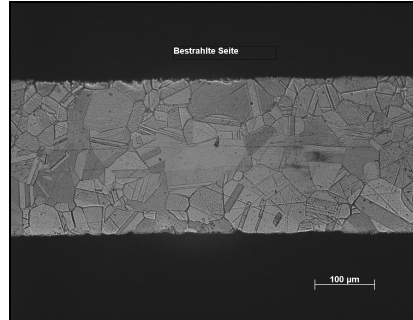
b

Fig. 9. Structure of the alloy A after 700 hr exposure in the molten salt under irradiation at $T=650^{\circ}C$ with the deposited energy (a) $E_d=5066\,eV/at$ and (b) $E_d=64\,ev/at$. Corrosion and precipitates within boundaries are larger at $E_d=5066\,eV/at$

The metallography data show considerable dependence of the intercrystalline corrosion on the alloy composition (Fig. 11). The structure specimens of alloy B is changed not so much after irradiation to large (fig. 11,a) and smaller (fig. 11,b) doses. Twines and many precipitates in grain bulk are seen. The grain size occurs to be not depending on E_d. It is seen that the alloy B possessing an "optimized composition" really has much higher corrosion resistance than the alloy A. But the mechanical tests show tha the irradiation changes microstructure of the alloy B too.
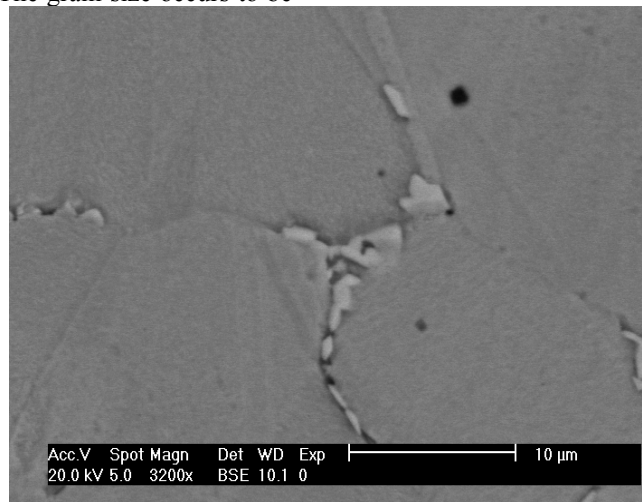

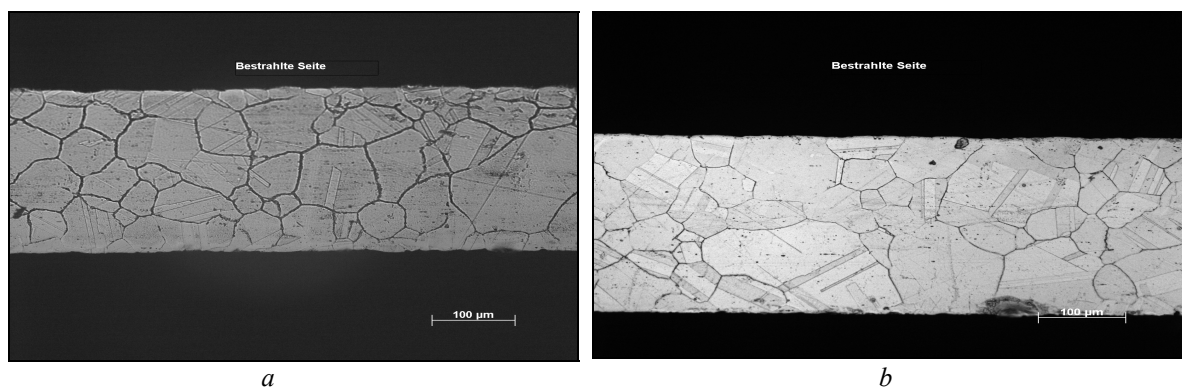Fig. 10. Precipitates within the grain boundaries of irradiated ($E_d=5066\,eV/at$) alloy A

ВОПРОСЫ АТОМНОЙ НАУКИ И ТЕХНИКИ. 2005. №.4.
Серия: Физика радиационных повреждений и радиационное материаловедение (87), с. 3-19.

11

| a | b |

Fig. 11. Structure of the alloy B after 700 hr exposure in the molten salt under irradiation at $T=650\,^{\circ}C$ *with the deposited energy (a)* $E_d=5066\,eV/at$ *and (b)* $E_d=64\,ev/at$ *. No considerable corrosion is seen*

4.5.2. CORROSION KINETICS AND COMPOSITIONAL CHANGES OF THE ALLOYS A AND B IN MOLTEN SALTS

The metallography data gives a macroscopic picture of the structural changes due to the corrosion of the alloys in molten salt. Investigations of compositional changes reveal peculiarities of the irradiation impact on the alloy recomposition under irradiation in molten salt. Dissolution of the components in salt and penetration of the salt constituents in specimen determine the corrosion kinetics. Voltammograms and corrosion current measurements are important characteristics of the corrosion determining the corrosion rate of material [15, 17-19].

An important characteristic of the corrosion is content of the dissolved elements in the salt. An informative parameter is the ratio of concentration of an element in salt to its concentration in alloy. When thermodynamic equilibrium is archived this ratio determines the equilibrium constant, K_i :

$$K_i = \frac{c_{i,l}^{salt}}{c_{i,l}^{alloy}} = \exp\left(-\frac{\mu_i^{salt}-\mu_i^{alloy}}{T}\right). \qquad (1)$$

Here $c_{i,l}^{salt}, c_{i,l}^{alloy}$ are the equilibrium concentrations, K_i is the equilibrium constant of ith element, and $\mu_i^{salt}, \mu_i^{alloy}$ are chemical potential of this element in salt and alloy respectively.

In the case that the system is not in the equilibrium the dissolution rate, dc_i^{salt}/dt , depends on the transport rate of ith element to the surface and the dissolution rate on the surface. The last one is proportional to $Sinh[(\mu_i^{alloy}-\mu_i^{salt})/T]$ while the transport rate strongly depends on phase structure and compositional heterogeneities of alloy. Considered in ref. [29] corrosion kinetics gives a constructive idea on the nature of these processes.

The compositional changes of the alloy A exposed in molten salt for 100, 200, 500 and 700 *hr* without irradiation revealed being in surface layers of 1…3 μm in the thick [15, 18].

Within the salt all main components of the alloy are revealed. The data on ratios c_i^{salt}/c_i^{alloy} are presented in Table 5. It has to be noted that we have at the moment a poor statistics and that the variance of the data obtained is unknown. Nevertheless one can conclude that without irradiation the basic elements Ni and Mo have rather low solubility in salt, $K_i<10^{-2}$. For Ti the equilibrium constant is also comparatively small, 2 ¿ 10^{-2} , while for Al it is 10 times larger. Evidently concentrations of Cr and Fe in the salt after 700hr are not saturated. Of course larger statistics is needed to get more accurate data.

Quantitative analysis of the salt composition after the test shows that the content of dissolved Ni, Mo, Al, Cr, Ti is small. An usefull parameter of corrosion kinetics is the ratio of an dissolved element content in salt and in alloy. These parameters are presented in Table 4.

Table 4

Element	Composition of alloy A, at. %	Ratio $\dfrac{c_{i,l}^{salt}\ at}{c_{i,l}^{alloy}\ at}$ after exposure in salt				K_i
		100 *hr*	200 *hr*	500 *hr*	700 *hr*	
Ni	81.041	0.00151	0.00022	0.00086	0.00108	1.23 10⁻⁵
Mo	7.578	0.00141	0.00141	0.00141	0.00141	1.84 10⁻⁴
Cr	7.808	0.00506	0.01772	0.00760	0.04295	
Fe	1.627	0.11303	0.18088	0.11313	0.24827	
Ti	0.148	0.03391	0.03392	0.03394	0.03385	0.23
Al	1.797	0.21194	0.21197	0.21211	0.21159	0.118

ВОПРОСЫ АТОМНОЙ НАУКИ И ТЕХНИКИ. 2005. №.4.
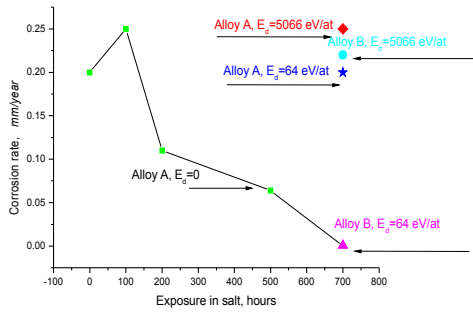*Серия:* Физика радиационных повреждений и радиационное материаловедение (87), с. 3-19.

12

Fig. 12. Corrosion rates of the alloy A and B depending on the exposure time in salt at 650 °C without and under e-irradiation at E_d= 5066 eV/at and E_d= 64 eV/at. The points depicted the corrosion rates of the unirradiated alloy A and irradiated alloy B at E_d= 64 eV/at with 700hr are overlapping

The corrosion rates of the alloy A in fresh molten salt after exposures 100, 200, 500 and 700 hr at $T = 650°C$ without irradiation and for alloys A and B after 700 hr under irradiation are presented in Fig. 12. It is seen that without irradiation the corrosion rate saturates on a rather low level $\sim 2 \dot{c} \ 10^{-4} mm/yr$. The presented in table 5 data are consisting with this conclusion but Cr and Fe dissolution are not saturated. For this reason the equilibrium constant for these elements is not determined. It is worth noting that applied electronic field in voltammetric measurements violets the equilibrium and that measured corrosion rate using this method can differ from that in absence of the electric field. Nevertheless the measured quantities can be accepted as reliable ones.
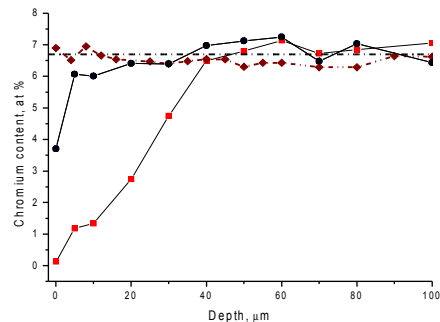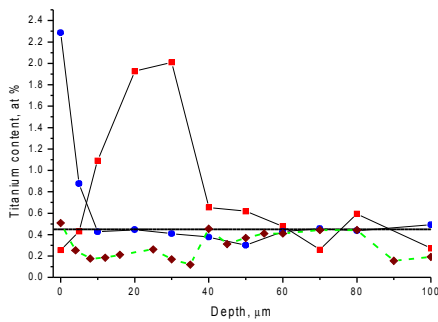

a

b

Fig. 13. Redistribution of a) Ti content and b) Cr content in surface layers of irradiated and non-irradiated samples after 700 hours exposure in salt (▯) –no irradiation; () – E_{dep} =64 eV/atom; () - E_{dep} =5066 eV/atom

The corrosion rate of irradiated in molten salt of alloy A is 0.1 $^{-4} mm/yr$ and is something higher for specimens with larger deposited energy E_d. The corrosion rate of alloy B to be essentially depending on E_d. It is $\sim 10^{-1} mm/yr$ at $E_d = 5066 \ eV/at$ while for $E_d = 64 \ eV/at$ it is $\sim 10^{-3} mm/yr$. This phenomenon have to be investigated in more detail but now one can conclude that the corrosion rate of alloy B in molten salt is sensitive to the deposited energy.

REMMA microanalysis and SIMS were used to investigate compositional changes of the surface layers of specimens. Results show considerable compositional heterogeneities in the surface layers. Ti heterogeneities and Cr, Al and Mo depletion zones were revealed in the surface layer. As example data on redistribution of Ti
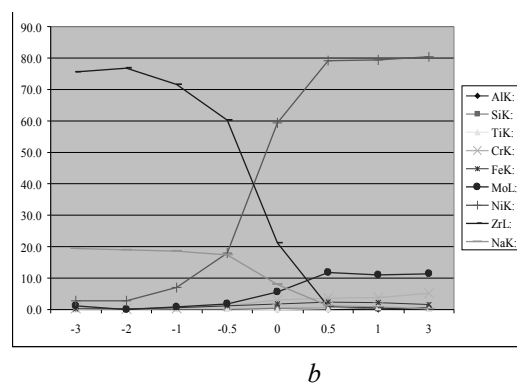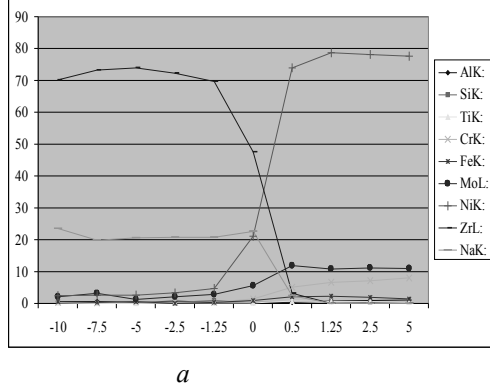
and Cr without and under e-irradiatrion in alloy A is shown in Fig. 13. Minor compositional changes are seen in samples after exposure in salt without irradiation. The scale and amplitude of compositional heterogeneities are depending on the deposited energy dose, E_d. Data of SIMS measurements are rather scattered but they clearly show that penetration depth of Zr and Na is depending on E_d [18]. Both of these elements are diffusing mainly in boundaries. A REMMA measurements data (Fig. 14) show that in a cavern within the grain boundary closely to the surface layer the salt is located and that Zr and Na penetrate in the grain of alloy A on 1.25 μm while the depth of these elements penetration is twice shorter in the case of alloy B at the same dose E_d = 5066 eV/at.

a

b

ВОПРОСЫ АТОМНОЙ НАУКИ И ТЕХНИКИ. 2005. №.4.
Серия: Физика радиационных повреждений и радиационное материаловедение (87), с. 3-19.

13

In bulk considerable compositional heterogeneities are seen in the vicinity of the grain boundaries (Fig. 15). Ni- Ti-precipitates enriched by and Si are forming with-

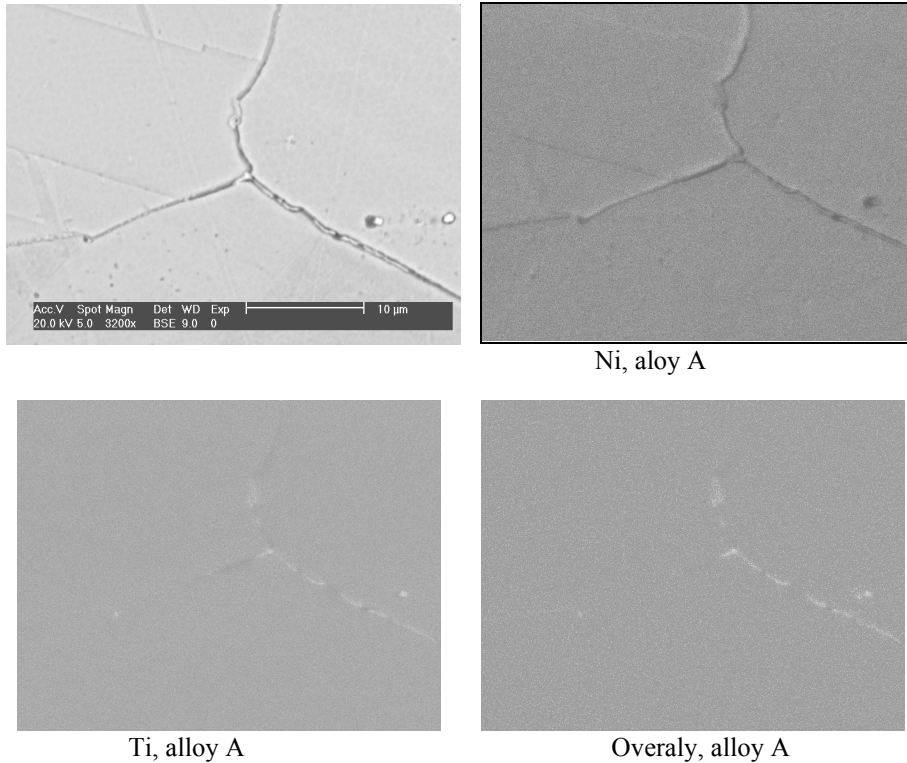in the boundaries and in grains. Average precipitate size depends on E_d

Ni, aloy A

Ti, alloy A

Overaly, alloy A

Fig. 15. Ni-Ti precipitates within grain boundaries of alloy A after 700 hr exposure in the molten salt at $T = 650^{\circ}C$ for 700 hr without irradiation [28]

It is worth noting that the variance of the compositional heterogeneities is rather large and that more careful investigation of them is needed to make a conclusion concerning impact of the irradiation on the alloy decomposition and corrosion kinetics. The precipitation kinetics also has to be investigated in more detail.

4.5.3. MECHANICAL PROPERTIES OF THE ALLOYS A AND B

The mechanical properties of reactor construction materials determine workability of the construction elements. The alloys A and B aged for 50hr at $T = 675^{\circ}C$ possess rather high (more than 50%) plasticity and yield stress σ_B , up to 1000 MPa at room temperature. At $T = 600^{\circ}C$ the yield stress of both alloys decreases on 50% while the plasticity threshold decreases much less, approximately on 25%. As result the plasticity is equal to 14% for alloy A and 19% for alloy B at $T = 600^{\circ}C$ [14]

Exposure of the alloy A in molten salt for 700hrs is resulting in increase of σ_B up to 20%. It is a result of the alloy aging and partial decomposition. The precipitates seen on the metallographic images, within grains and grain boundaries, increase in size.

The electron irradiation reduces both considerably σ_B and σ_{O2} of the alloy A and alloy B and the reduction is larger at $E_d = 5066\,eV/at$ than at $E_d = 64\,eV/at$. At the same time, the plasticity does not depend on composition and deposited energy, at $T = 650^{\circ}C$, $\delta = 15$.

In ref.[5] data of mechanical tests of alloy U, which in composition differs not so much from alloy B, are reported. This alloy was exposed to neutron irradiation in nitrogen atmosphere with neutron energy more than 0.5 Mev and flux 4 10²⁰ neutron/cm². As result the alloy was strengthened as compare to unirradiated material but its plasticity decreases from 59.2 to 33.3 at $T = 650^{\circ}C$. At the moment we have not enough experimental data on impact of neutron irradiation on Ni-Mo alloys to compare with our data.

Nanoidentation gives an additional information on impact of aging, molten salt and irradiation on the alloys. A typical size of nanoindentor imprint is 50 *nm*. Therefore the nanoindentation allows to measure hardness and Young modulus of rather small regions. If compositional and structural heterogeneities have scale larger than the indenter imprint, changes of the properties due to these heterogeneities can be revealed.

ВОПРОСЫ АТОМНОЙ НАУКИ И ТЕХНИКИ. 2005. №.4.
Серия: Физика радиационных повреждений и радиационное материаловедение (87), с. 3-19.

14

An example of irradiated with $E_d = 64\,eV/at$ specimen of the alloy A after nanoindentation is shown in Fig. 16 [30].

Revealed impact of e-irradiation on the surface and intercrystalline corrosion tells not so much on changes within grains and specimen bulk. Measurements performed show that Young modulus of both alloys A and B irradiated and unirradiated in molten salt are very the same, in bulk E ≈ 240 GPa and that these quantities are not sensitive to the dose deposited energy. Both H_μ and E considerably decrease in the surface layer. The width of this layer is 3…5 μm without irradiation and 7…15μm for irradiated specimens. At the same time, the hardness the unirradiated specimens exposed in salt for 700hr increase, in bulk H_μ ≈ 6 GPa. For irradiated specimens of the alloy A this quantity is H_μ ≈ 4.3 GPa and for the alloy B H_μ= 5 GPa. It occurs that the nanohardness is sensitive to the alloy composition but it is not sensitive to the dose of the deposited energy. Possible the dose effect saturates at E_d > 60 ev/at.
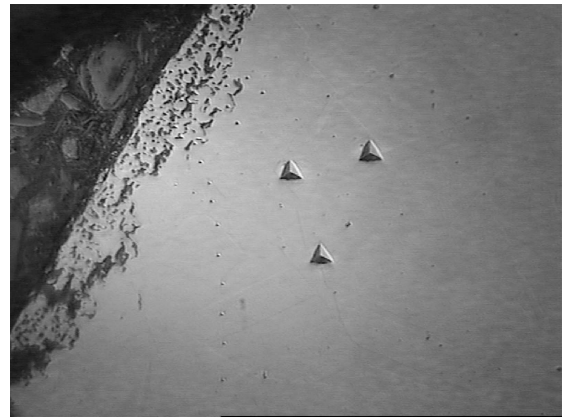

Fig. 17. SEM of corroded surface layer of the alloy A after exposure for 500hr in molten salt with La impurities at $T = 600\,^\circ C$ *. Three large imprints are marks of the investigated area. A row of small imprints of the nanoindentor are seen*
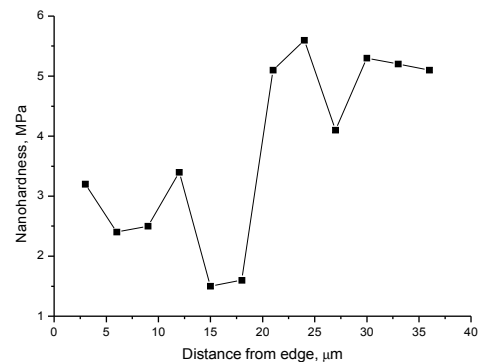
The nanohardness measurement data are shown in Fig. 18.

Fig. 18. Depth dependence of the nanohardness of the specimen shown in Fig. 17 [30]

Fig. 16. Surface layer of the alloy A irradiated in salt with $E_d = 64\,eV/at$ *. Intercrystalline cracks and indentor imprints are seen*

Worth noting is that nanohardness correlates with the yield stress and σ_{O2} of specimens.

It occurs that small addition of La (wt%) in salt considerably changes the corrosion rate and nanohardness of the alloy A [19]. In this case the nanoindentations allows determine the width of corroded layer very well. In Fig. 17 the structure of surface layer of the alloy A after exposure in molten salt with La impurities for 500hr at $T = 600\,^\circ C$. It is seen that the corrosion stroked the sample on depth 20…25 μm.

4.8. PROTECTIVE W- AND MO- COVERS

It was found that the Hastelloys are not corrosion resistant in molten metals: lead, lead-bismuth eutectics and bismuth. For example, in the molten Bi the standard specimen of alloy A was dissolved for 300 *hr* at T = 550 °C. Tungsten and molybdenum are known as corrosion resistant materials in the mentioned metallic coolants. These metals were used as protective covers of the alloy A [31]. We aware that these covers would be more efficient on alloys possessing higher corrosion resistance, e.g. ferritic-martensitic steels. Nevertheless the alloy with poor corrosion resistance was used to check quality of the covers. Indeed, if a cover is penetrable for Pb or Pb-Bi than the substrate will be dissolved after exposure in the melt. It is possible that the alloy components (Ni, Cr, etc.) penetrate trough the cover but this process is much slower than dissolution of the alloy contacting with melt.

Samples of the alloys with W and Mo coatings (coating thickness 60 and 90 μm) were soaked at 550 °C for over 300 hours in molten metals in absence of oxygen. The state of the samples Pb and Pb-Bi melts was satisfactory. No traces of corrosion were observed visually. No mass loss was noted either. A microsection of

ВОПРОСЫ АТОМНОЙ НАУКИ И ТЕХНИКИ. 2005. №.4.
Серия: Физика радиационных повреждений и радиационное материаловедение (87), с. 3-19.

15

tungsten-coated sample of composition A after contact with molten lead is shown in Fig. 19.

Hastelloy

Tungsten coating

Copper holder

In the Bi melt bath, as it was noted, the uncoated specimens of alloys A and B dissolved completely for 300 hours while the coated samples were not corroded considerably. The percentage of the alloy components in melts after exposure of the alloy A specimen covered by W is given in Table 4.

Table 4

Percentage of the alloy constituents in molten metals-coolants

Alloy constitu- ent	Percentage in the original alloy	Percentage in the metal melt bath		
		Pb	Pb–Bi	Bi
Ni	78.15	0.016	0.0241	0.225
Fe	1.5	0.019	0.0185	0.013
Cr	6.7	0.004	0.005	< 0.003

After the isothermal soaking of alloy samples in molten metals, microsections were made, and nanohardness was measured. The results are following. No change in hardness has been observed in coating or al-loy of the samples soaked in a molten lead-bismuth eutectic (Fig. 20). Very the same results were observed for the covered alloys specimens after exposure in a molten lead-bismuth eutectic.
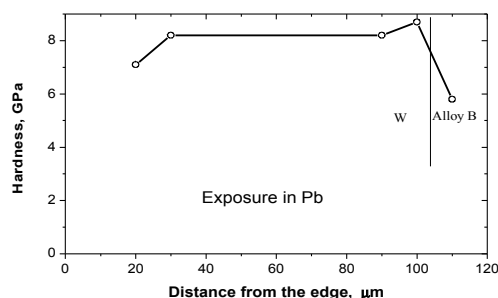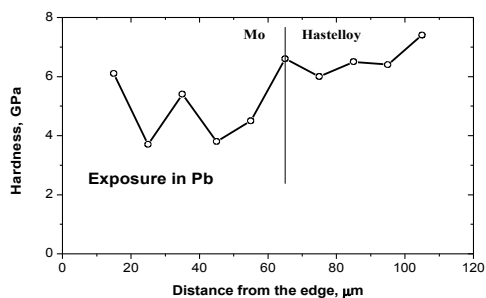

Fig. 20. Nanohardness of molybdenum-coated samples of alloy A (above) and tungsten-coated samples (below) after contact with molten lead for 300 hours

X-ray microanalysis shows that lead does not penetrate either into the coating or into the alloy. Traces of lead get onto the surface of sample during its polishing. In the coated samples, a redistribution of both the main alloy constituent (nickel and molybdenum) and the alloying constituents is observed at the coating-alloy interface. In Fig. 21 and Fig. 22 distributions of Ni and Fe in covers are shown. It is seen that these components considerably diffuse in covers. The diffusivity of Ni in Mo and W is very the same while Fe in W diffuses faster than in Mo. For this reason a depleted Fe zone is formed in the alloy A in the vicinity of interface. The data of chemical analysis of the melts after exposure of covered specimens (Table 4) confirm this conclusion. Thus these tests show that the W and Mo covers were of good quality and that these materials can be used for protection of materials from corrosion in molten fluoride salts.
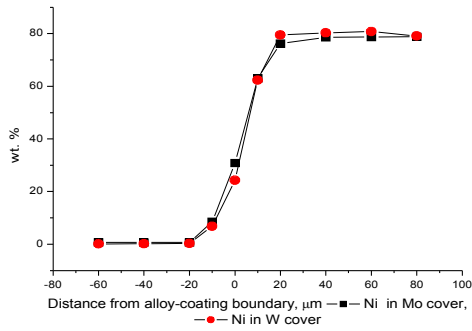
ВОПРОСЫ АТОМНОЙ НАУКИ И ТЕХНИКИ. 2005. №.4. *Серия:* Физика радиационных повреждений и радиационное материаловедение (87), с. 3-19.

16

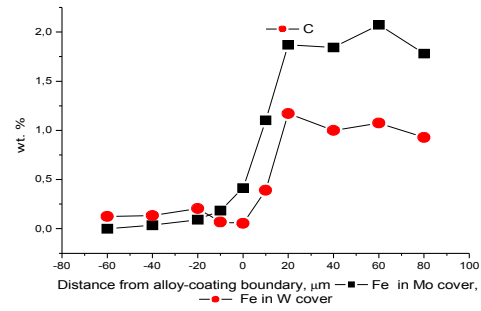Fig. 21. Distributions of Ni in Mo and W covers and in alloy A

Fig. 22. Distribution of Fe in Mo and W covers and in alloy A

4.9. PILOT TESTS OF A STEEL USING USTF

Full-scale tests of irradiated and unirradiated specimens of alloys A and B will be done in the near future. Currently we have performed some pilot tests of different materials to check efficiency of the constructed USTF. The tests show that the used ultrasound impacts considerably the mechanical properties of alloys even at room temperature [16]. The ultrasound generator output power was 3,5±0,5 kw but the amplitude of the specimen ultrasonic vibrations was not measured due to lacking of a proper tools. An example of the pilot measurements is presented in Fig. 23.
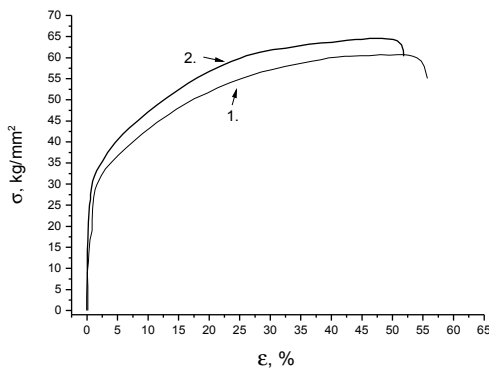

Fig. 23. Strain-stress curves of the stainless steel X18H10T (Cr – 18%, Ni – 10%, Ti – 0.45%) (1) without and (2) with impact of ultrasound at room temperature. The strain rate was nearly 0.15 min^{-1}

It is seen that a strengthening and a decrease of plasticity (from 55 to 50%) takes place in result of the ultrasound action. Usually a strengthening of material appears due to multiplication and pinning of dislocations. It is likely that an additional pinning of dislocation is caused mainly by vacancy complexes generated by the ultrasound [32-34].
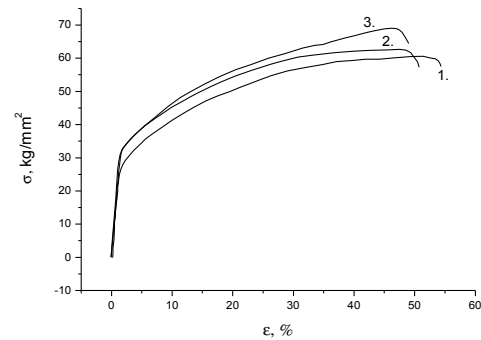

Fig. 24. Strain-stress curves (1) without and (2,3) with impact of ultrasound at room temperature. The strain rate was nearly 0.15 min^{-1} in absence at the ultrasound, (curve 1). It was equal to 0.15 min^{-1} (curve 2) and 0.009 min^{-1} (curve 3) at ultrasound vibrations

In Fig. 24 are shown the stress-strain curves without sound impact (curve 1) at a large strain rate ($d\varepsilon/dt$ = 0.15 min^{-1}) and under ultrasound action at smaller stain rate, $d\varepsilon/dt$ = 0.03 min^{-1} (curve 2) and $d\varepsilon/dt$ = 0.009 min^{-1} (curve 3). The ultrasound generator output power was nearly twice less then in previous measurements shown in Fig. 23. One can see that the specimen hardening and the plasticity loss due to the ultrasound action increases when the strain rate decreases. This result is expected because generation of vacancies and multiplication of dislocations (if the last one happens) takes place for a longer time at slower deformation. For this reason the density of the generated by ultrasound defects is larger for smaller strain rates.

Performance of full-scale experiments and investigations in a wide temperature range have to be made to study the microscopic nature of the observed phenomena. Especially interesting is issue on difference of mechanical properties of irradiated and unirradiated specimens under ultrasonic vibrations.

4.10. THEORETICAL MODELS OF KINETIC PROCESSES UNDER IRRADIATION

Without irradiation a nonequilibrium conservative system relaxes approaching the stable equilibrium state. Thermodynamic driven forces and thermal activations determine the kinetics of relaxation. A system under ir-

ВОПРОСЫ АТОМНОЙ НАУКИ И ТЕХНИКИ. 2005. №.4.
Серия: Физика радиационных повреждений и радиационное материаловедение (87), с. 3-19.

17

radiation is non-conservative. For it the equilibrium states and relaxation kinetics have to be described within frameworks of properly developed models. Kinetic coefficients of these models depend on both thermodynamic and irradiation parameters.

Corrosion of multicomponent alloys in molten salts or metallic coolants is a complicate process including transport of components, dissolution and a wide spectrum of chemical reactions. An irradiation is resulting in local strong damages (generation of the Frenkel pairs, formation of the displacement cascades, compositional replacements of atoms) and soft damages (generation of unstable Frenkel pairs, excitations of atoms). In our experiments the electron and x-ray irradiation produces mainly soft damages which impact considerably the corrosional kinetics on the interface alloy-melt.

Features of the kinetic processes on interfaces under electron irradiation are investigated, taking as example amorphization of Zr Fe precipitates under electron irradiation, in ref [36]. This example was chosen because it was investigated experimentally [37]. A theoretical model proposed in [38] is based on assumption that just the strong damages, Frenkel pairs and compositional disordering, are responsible for this phase transformation. It is shown in [36] that the soft damages can enforce the amorphization inspite in this case the thermodynamically stable crystalline phase transforms into metastable amorphous state. This example shows that the soft radiation damages can even change the direction of the phase transformation and therefore they can considerably impact the corrosion of alloys in metals. The stored experimental data on corrosion under irradiation are yet not enough to develop a proper quantitative description of this processes but a progress in its understanding is made.

Corrosion rate of a metal in molten metallic coolant depends on its solubility, coolant velocity, surface structure etc. To decrease the corrosion rate, protective covers are useful. As it is known, in Pb and PBE coolants protective oxide layers covering the metal surface, are efficient (see e.g. [39] and references quoted). If the coolant is saturated by oxygen then the oxide layer can grow permanently on the surface of metal contacting with the coolant. Therefore description of the kinetics of a metal with covered by an oxide surface layer and kinetics of the oxide growth is a problem of great interest. In ref. [29] this problem is considered within the framework of proposed there kinetic equations.

The metal atoms diffuse through the oxide layer and dissolve in molten coolant due to a difference of the chemical potential of the atoms in the metal and solution. Due to the vacancy mechanism of diffusion, the currents of metal atoms and vacancies are equal in absolute value and excess vacancies are pouring into the metal. Therefore the kinetics of both metal atoms and vacancies have to be considered to determine the corrosion rate.

If occurs that the corrosion current of metal atoms is equal to

$$|j_m| = \sqrt{\frac{D_{vm}^{ox} c_{vm}^{\overline{ox}}}{L_{ox}} \frac{D_m^{Pb} c_m^{\overline{Pb}}}{L_m}} \qquad (2)$$

The width of the oxide layer is L_{ox} and L_m is the width of diffusional region of the metal atoms within the coolant; D_{vm}^{ox} is the diffusion coefficient and $c_{vm}^{\overline{ox}}$ is the equilibrium concentration of the metallic vacancies within the oxide; D_m^{Pb} and $c_m^{\overline{Pb}}$ is the diffusion coefficient and equilibrium concentration of the metal atoms in the coolant.

To describe the growth kinetics of oxide the diffusional transport of both metal and oxygen atoms are taken into account. The growth rate is proportional to $\sqrt{t}$ in all cases but the proportionality coefficient depends on the oxide layer width, diffusion coefficients, chemical potentials, etc.

It is shown [29] that at a high concentration of oxygen in the coolant the oxide layer growth can be blocked due to formation of nuclei of a complex oxide including atoms of both metal and coolant. It seems that this phenomenon was observed in some experiments [40].

In the theoretical models developed in [29] the irradiation role on the kinetics is not yet taken into account but the results obtained can be helpful for analysis of the big amount of data of experiments performed in loops without of an irradiation.

5. DISCUSSION

Inspite the Ni-Mo alloys possess good corrosion resistance in molten salts the stored up to now data [4-6] do not allow to select a best alloy for long-term use in MSR. Our data show that

– irradiation considerably impacts the corrosion;
– corrosion resistivity is rather sensitive to comparatively small compositional changes. The alloys A and B have minor composition difference but their corrosion resistivity without and under irradiation are considerably different. Beside, the corrosion rate of alloy B is more sensitive to the deposited energy E_d;
– impurities of La in the ZrF$_4$-NaF molten salt enhance the corrosion of the alloy A even without irradiation.

The results obtained show that systematic investigations of corrosion of Ni-Mo alloys of different compositions in molten salts containing fluorides of actinides, lanthanides and other impurities expected to appear in blanket of MSR is severely needed . An interesting issue is dependence of Ni-Mo alloys corrosion dependence on Nb and other impurities content. In ref [6] a lot of data on dependence of Ni-Mo alloys corrosion on different alloying elements are published. These data form a good base for tests of corrosion similar alloys under irradiation.

The fact that C-C composite occurred to be rather resistant to corrosion and to impurity penetration in molten salt as well as in Pb and PBE melts at long-term exposure shows that this material is a good candidate

ВОПРОСЫ АТОМНОЙ НАУКИ И ТЕХНИКИ. 2005. №.4.
Серия: Физика радиационных повреждений и радиационное материаловедение (87), с. 3-19.

18

for MSR and ADTS. Workability of the composite is rather good but its functional properties in specified reactor conditions, especially its mechanical properties, have to be investigated in more detail. It is desirable to test the C-C composites at more hard condition including higher temperature (above 1000 $^\circ C$), larger deposited energy and carbide forming impurities to make clear under which conditions this material can be used.

A correlation of the nanohardness and yield stress of the irradiated specimens is revealed in the performed measurements. Similar correlation of microhardness and yield stress of irradiated alloys was demonstrated in ref. [35]. Inspite that a poor data base on this correlation is stored, it is believed that the nanoindentations can be used for semi quantitative estimations of the macroscopic mechanical properties of irradiated materials.

The specimens of alloy A and B covered by W and Mo films have considerably better corrosion resistance in Pb and PBE melts than the uncovered specimens do. Besides the W and Mo covers are impenetrable for Pb and Bi. From other side atoms of Ni and Fe, being components of the alloys A and B, penetrated in the covers on large depth for 300 hr. It means that composition of steel under W or Mo cover has to be thoroughly chosen to diminish solubility of Ni and Fe in covers and transportation of these elements into metallic coolant through covers. First of all the ferritic-martensitic steels, showing acceptable corrosion resistance in molten Pb and PBE, and modified by impurities steels of this family have to be used as basic alloys for covers. It is interesting to compare protective properties of oxide films and W,Mo covers of steels in molten Pb and PBE.

An important issue is to make clear to which measure the corrosion processes of the materials tested under electron irradiation are simulating impact of neutron irradiation on the corrosion in molten salts and metallic coolants. For that additional tests are needed. Anyway one can expect that the results of tests under electron irradiation correlate with those under neutron irradiation and that comparatively fast tests using EITF should be very useful for design and selection of advanced materials for MSR and ADTS.

6. CONCLUSIONS

- EITF is an efficient irradiation tool for corrosion tests of ADTT candidate construction materials.
- No visible changes of macroscopic mechanical, nano-plastic, compositional properties or corrosion resistance of C-C composite material fabricated in NSC KIPT were found after long contact with molten fluoride or metallic coolants.
- Both irradiation ampoules and test samples from C-C composite show no changes of properties.
- C-C material is therefore proposed for use in construction of ADTT.
- Hastelloy alloys A and B have good corrosion resistance in fluoride salt at 650°C. Voltamperic measurements show that the corrosion rate of both alloys is

negligible after 700 hour exposure without irradiation.
- After electron irradiation in EITF for 700 hours the voltamperic data provide a preliminary estimation of the corrosion rate to be ~ 0.1 mm/year.
- Changes of the strength and yield stress of the Hastelloys after e-irradiation in salt in EITF are similar to those observed in samples after fast neutron irradiation to dose 3·1020 cm^{-2} at 650°C.
- These results show that the tools and methods developed in this program can be used for tests of metallic alloys of different compositions, castings and thermal treatments.
- The deposition methods developed for W and Mo coatings ensure corrosion protection coatings which are resistant to attack in metallic coolants.
- To make clear to which measure the corrosion processes of the materials tested under electron irradiation are simulating impact of neutron irradiation on the corrosion in molten salts and metallic coolants additional reactor tests are needed.

ACKNOWLEDGEMENT

REFERENCES

1. US Department of Energy sponsored study, *A Technical Roadmap for Generation IV Nuclear Systems: Technical Roadmap Report*, Washing5ton DC, October, 2002.
2. *Power provision of mankind sustainable development, cardinal solution of the nuclear weapons non-proliferation problem, and the problem of the environmental recovery of the Earth Planet*, IAE- 6213/3 Kurchatov Institute, Moscov, 2001.
3. J. Vergnes. The AMSTER Concept //6th OEDC/NEA *information exchange meeting on actinide and fission product portioning and transmutation, Madrid, Spain*, 2000.
4. P.N. Haubereich, J.R. Engel. Expirience with molten salt reactor experiment //Nucl. Appl. Technol. 1970, v. 8, p. 118–136.
5. V.M. Novikov, V.V. Ignat'ev, V.I. Fedulov, V.N. Cherednikov. *Molten Salt Nuclear Energy Systems – Perspective and Problems*. Moskva: "Energoatomizdat", 1990 (in Russian).
6. J.H. DeVan. Effect of alloying additions on corrosion behaviour of nicel-molibdenum alloys in fused fluoride mixtures //ORNL Report ORNL-TM-2021, 1969.
7. G.S. Yachmenov et al. Problems of structural materials corrosionin lead-bismuth coolant //*Proc. of Heavy Liquid Metal Coolants in Nuclear Technology, Obninsk (Russia).*1999, p. 133.
8. I.V. Gorynin et al. Structural materials for power plants with liquid metals as coolant in: Proc. of Heavy Liquid Metal Coolants in Nuclear Technology, Obninsk, (Russia), 1999 p. 120.
9. F.A. Garner. Materials breakout group summary //*Proc. of Second Int. Conf. on Accelerator-driven*

ВОПРОСЫ АТОМНОЙ НАУКИ И ТЕХНИКИ. 2005. №.4.
Серия: Физика радиационных повреждений и радиационное материаловедение (87), с. 3-19.

19

Transmutation Technologies (Kalmar, Sweden, 1996), Upsala University, 1996, p. 1161–1162.

10. V.M. Azhazha, A.S. Bakai, I.V. Gurin et al. Electron irradiation test facility for irradiation of structural materials for molten salt reactors (in this volume).

11. O.S. Bakai, M.I. Bratchenko, S.V. Dyuldya. *Electron beams transport and energy deposition in heterogeneous assemblies of the Hastelloy samples embedded into the molten salt fluorides mix* (in this volume).

12. O.S. Bakai, L.V. Tanatarov, V.Yu. Gonchar and G.G.Sergiyeva. *Calculation of temperature fields in ampoules under irradiation treatment by electrons with energy 10 MeV* (in this volume).

13. M.J. Berger. *ESTAR, PSTAR, ASTAR — A PC package for calculating stopping powers and ranges of electrons, protons and helium ions*. NIST Report NISTIR-4999, 1993. (IAEA-NDS-144, 1993).

14. V.M. Azhazha, A.S. Bakai, A.N. Dovbnya et al. *The effects of electron irradiation and fluoride salt melt $ZrF_4 - NaF$ on mechanical properties of Hastelloy N type alloys* (in this volume).

15. V.M. Azhazha, A.A. Andriiko, A.S. Bakai et al. *Corrosion of irradiated Ni-Mo alloys in sodium fluoride – zirconium fluoride melt* (in this volume).

16. A.S. Bakai, S.A. Bakai, G.N. Malyk, V.M. Gorbatenko, V.M. Netesov, V.A. Yemlyaninov. *Ultrasonic test facility for investigation of ultrasound impact on mechanical properties of materials* (in this volume).

17. V.M. Azhazha, A.S. Bakai, Yu.P. Bobrov et al. *The corrosion resistance of heatproof nickel alloy in molten fluoride salts* (in this volume).

18. V.M. Azhazha, A.S. Bakai, Yu.P. Bobrov et al. *Variation of compositional content in subsurface layers of Hastelloy type alloys as caused by melt of fluorides $ZrF_4 - NaF$ and electron irradiation* (in this volume).

19. A.S. Bakai, S.V. Volkov, V.M. Azhazha et al. *Corrosion Processes in Zirconium Fluoride – Sodium Fluoride Melts. Study of Shortcut Cell $C/(ZrF_4 - NaF)_{eut}/Hastelloy$* (in this volume).

20. A.S. Bakai, A.N. Dovbnya, A.I. Zykov et al. *Nuclide control of structural materials tested in electron irradiation test facility* (in this volume).

21. A.S. Bakai, A.A. Borisenko, K.C. Russell. *On kinetics of crystall amorphysation under electron irradiation* (in this volume).

22. A.S. Bakai, L.V. Tanatarov (in this volume).

23. A.A. Andriiko, A.A. Omelchuk, A.S. Bakai. *Reaction of zirconium with alkali halide melts* (in this volume).

24. V.M. Azhazha, O.S. Bakai, I.V. Gurin et al. *Electron Irradiation Test Facility for irradiation of structural materials in conditions of molten salt reactor* (in this volume).

25. V.A. Gurin, O.S. Bakai, I.V. Gurin et al. *Structural carbon-carbon materials for accelerator-driven systems* (in this volume).

26. W.C. Oliver and G.M. Pharr. An improved technique for determining hardness and elastic modulus using load and displacement sensing indentation experiments //*J. Mater. Res.* 1992, v. 7, #6, p. 1564–1583.

27. N. Iwashita, J.S. Field, M.V. Swain, Indentation hysteresis of glassy carbon materials // *Phil. Mag.* (82). 2002, #10, p. 1873–1881.

28. A.S. Bakai, N. Wanderka, H. Kropf et al. (unpublished).

29. A.S. Bakai, L.V. Tanatarov. Corrosion kinetics of an alloy immerged into a molten metal containing oxygen, (in this volume).

30. A.S. Bakai, S.N. Dub, A.A. Omelchuck et al. (unpublished).

31. V.M. Azhazha, O.S. Bakai, P.I. Glushko et al. *Corrosion stability of molybdenum and tungsten coatings in lead-bismuth eutectic* (in this volume).

32. A.V. Kulemin. *Ultrasound and diffusion in metals*. Moscow: "Metallurgia", 1978.

33. A.S. Bakai and N.P. Lazarev. Effect of sound on diffusion in solids //*Sov. Phys. Solid State.* 1984, v. 26, p. 1517.

34. A.S. Bakai and N.P. Lazarev. Effect of acoustic waves on the diffusion of interstitial impurity atoms in a solid //*Sov. Phys. Solid Stat.* 1986, v. 28, p. 1373.

35. J.T. Busby, M.C. Hash, G.S. Was. The relationship between hardness and yield stress in irradiated austenitic and ferritic steels //*J. Nucl. Mater.* 2005, v. 336, p. 267–278.

36. A.S. Bakai, A.A. Borisenko, K.C. Russell. On kinetics of crystal amorphization under electron irradiation, (in this volume)

37. A.T. Motta, L.M. Howe, P.R. Okamoto //*Journal of Nuclear Materials.* 1999, v. 270, p. 174.

38. A.T. Motta, D.R. Olander //Acta Met. 1990, v. 38, p. 2176

39. Ning Li. Active control of oxygen in molten lead-bismuth eutectic systems to prevent steel corrosion and coolant contamination //*Journal of Nuclear Materials.* 2002, v. 300, p. 73–81.

40. O.I. Eliseeva, V.M. Fedirko, Ya.S. Matychak, V.P. Tsysar. Interaction of solid metals with melts containing nonmetallic impurities //*Fiziko-khimicheskaya mekhanika materialov.* 2000, # 5, с. 69–76 (in Ukrainian).

ИССЛЕДОВАНИЕ МАТЕРИАЛОВ ДЛЯ ЖИДКОСОЛЕВЫХ РЕАКТОРОВ И РЕАКТОРОВ С Pb-Bi ОХЛАДИТЕЛЕМ С ПОМОЩЬЮ ЭЛЕКТРОННОГО ОБЛУЧАТЕЛЬНОГО ИСПЫТАТЕЛЬНОГО СТЕНДА

В.М. Ажажа, А.С. Бакай, И.В. Гурин, И.М. Неклюдов, А.А. Омельчук, В.Ф. Зеленский, Ф. Гарнер

Приведен обзор результатов, полученных в рамках проекта УНТЦ № 294.

ДОСЛІДЖЕННЯ МАТЕРІАЛІВ ДЛЯ РІДКОСОЛЬОВИХ РЕАКТОРІВ ТА РЕАКТОРІВ З Pb-Bi ОХОЛОДЖУВАЧЕМ ЗА ДОПОМОГОЮ ЕЛЕКТРОННОГО ОПРОМІНЮВАЛЬНОГО ВИПРОБУВАЛЬНОГО СТЕНДУ

В.М. Ажажа, О.С. Бакай, І.В. Гурін, І.М. Неклюдов, А.О. Омельчук, В.Ф. Зеленський, Ф. Гарнер

Наведено огляд результатів, отриманих в рамках проекту УНТЦ № 294.

ВОПРОСЫ АТОМНОЙ НАУКИ И ТЕХНИКИ. 2005. №.4.
Серия: Физика радиационных повреждений и радиационное материаловедение (87), с. 3-19.

20